

Quantitative Imaging of Iodine-124 with PET

Keith S. Pentlow, Martin C. Graham, Richard M. Lambrecht, Farhad Daghighian, Stephen L. Bacharach, Bernard Bendriem, Ronald D. Finn, Kurt Jordan, Hovanes Kalaigian, Joel S. Karp, William R. Robeson and Steven M. Larson
Departments of Medical Physics and Radiology, Memorial Sloan-Kettering Cancer Center, New York, New York; North Shore University Hospital, Manhasset, New York; National Institutes of Health, Bethesda, Maryland; Brookhaven National Laboratory, Upton, New York; Medizinische Hochschule Hannover, Hannover, Germany; Hospital of the University of Pennsylvania, Philadelphia, Pennsylvania; King Faisal Specialist Hospital and Research Center, Riyadh, Saudi Arabia

PET is potentially very useful for the accurate in vivo quantitation of time-varying biological distributions of radiolabeled antibodies over several days. The short half-lives of most commonly used positron-emitting nuclides make them unsuitable for this purpose. Iodine-124 is a positron emitter with a half-life of 4.2 days and appropriate chemical properties. It has not been widely used because of a complex decay scheme including several high energy gamma rays. However, measurements made under realistic conditions on several different PET scanners have shown that satisfactory imaging and quantitation can be achieved. **Methods:** Whole-body and head-optimized scanners with different detectors (discrete BGO, block BGO and BaF₂ time-of-flight), different septa and different correction schemes were used. Measurements of resolution, quantitative linearity and the ability to quantitatively image spheres of different sizes and activities in different background activities were made using phantoms. **Results:** Compared with conventional PET nuclides, resolution and quantitation were only slightly degraded. Sphere detectability was also only slightly worse if imaging time was increased to compensate for the lower positron abundance. **Conclusion:** Quantitative imaging with ¹²⁴I appears to be possible under realistic conditions with various PET scanners.

Key Words: PET; iodine-124; quantitative imaging

J Nucl Med 1996; 37:1557-1562

Radionuclides of iodine are widely used in nuclear medicine to label monoclonal antibodies, receptors and other pharmaceuticals in diagnostic and therapeutic applications where quantitative imaging over a period of several days is necessary (1-4). Unfortunately, the nuclides most commonly used, ¹²³I, ¹²⁵I and ¹³¹I, all have limitations. Iodine-123 has too short a half-life, if the pharmaceutical is to be followed over several days. Iodine-125 has a photon energy too low for optimal imaging, especially quantitative imaging, and its half-life is undesirably long. Iodine-131, the most widely used of the three, has a photon energy which is too high for optimal imaging. Furthermore, SPECT imaging does not permit a rigorous attenuation correction, although a satisfactory empirical correction may sometimes be achieved (5-7). Iodine-124, a positron-emitting nuclide with a half-life of 4.2 days, could permit quantitative imaging over several days using PET. Iodine-124, however, has a complex decay scheme (Fig. 1) (8). Only about 23% of disintegrations result in positron emission and these are of relatively high energy. There are also many high-energy gamma rays, some in cascade with the positron emissions. (The term "gamma rays" here and elsewhere in this article implies photons emitted from the nucleus. Photons resulting from positron-electron annihilations are termed "annihilation photons").

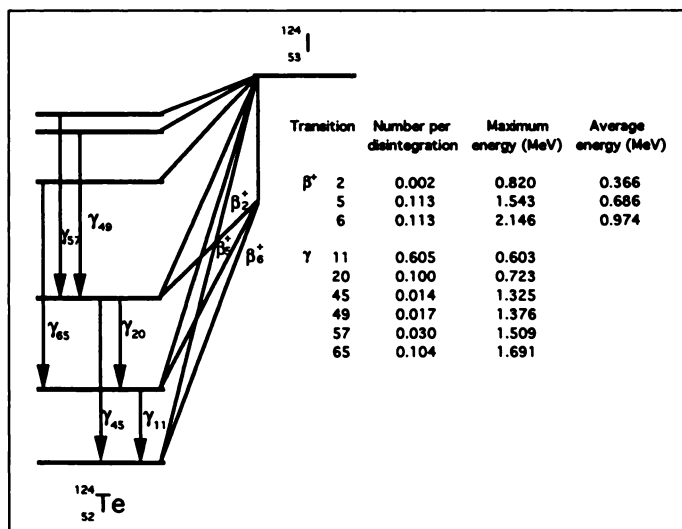


FIGURE 1. Simplified decay scheme of ¹²⁴I. MIRDB (8) indicates at least 25 electron capture transitions, 6 positron transitions and 97 gamma-ray transitions. Numbering of transitions follows this reference. Omitted transitions are each less than 1% per disintegration. Only about 23% of disintegrations result in positron emission while the gamma ray abundance exceeds 90% per disintegration.

Given such a decay scheme, ¹²⁴I was, for many years, largely ignored or considered unsuitable for PET imaging. Recently, its use for imaging and for potentially quantitative applications has been growing (9-21).

In an earlier phantom study, it was shown to be possible to image satisfactorily and quantitatively with ¹²⁴I under conditions similar to those likely to be encountered with agents such as monoclonal antibodies in humans (22). Because there are significant differences in design between many of the scanners in use today which may affect their ability to image ¹²⁴I, the present study was carried out to determine whether quantitative imaging could be performed using representative modern scanners. The study is not a performance comparison of the various scanners.

MATERIALS AND METHODS

Scanners

The various PET scanners (23-26) used in this study, together with differences in features that may potentially affect imaging performance with ¹²⁴I, are listed in Table 1. Some acquisition parameters, reconstruction parameters, and correction schemes may be determined by the operator at the time of the scan. Those used for imaging phantoms in this study are listed in Table 2.

Radionuclide Production

The ¹²⁴I was produced on a CS-30 cyclotron (Cyclotron Corp.) at the King Faisal Specialist Hospital, Riyadh, Saudi Arabia and shipped by air to the United States or Germany. The ¹²⁴Te (d,2n)

Received May 13, 1994; revision accepted Feb. 7, 1996.

For correspondence or reprints contact: Keith S. Pentlow, MSc, Department of Medical Physics, Memorial Sloan-Kettering Cancer Center, 1275 York Ave., New York, NY 10021.

TABLE 1
Summary Specifications of Scanners Used in This Study: Differences That May Potentially Affect Imaging with Iodine-124

	Cyclotron Corp. PC4600	Positron Corp. Posicam	Scanditronix SP3000	Siemens/CTI ECAT 931	Siemens/CTI ECAT 951
Field of view	Head	Body	Body	Body	Body
Ring diameter	60 cm	78 cm	90 cm	102 cm	102 cm
Detector type	Discrete BGO	Staggered BGO	BaF ₂ time-of-flight	Cut block BGO	Cut block BGO
Crystal to PMT ratio	1:1	2:1	1.6:1	8:1	16:1
Number of detector rings/planes	5/9	11*/21	4/7	8/15	16/31
Cross-planes used	1st order	4th order	1st order	1st order	3rd order
Inter-plane septa	Four 3 mm × 13 cm tungsten	Ten 1.5 mm × 7 cm lead	Three 1.25 mm × 16.5 cm tungsten	Seven 1 mm × 18.5 cm tungsten	Fifteen 1 mm × 7 cm tungsten
Energy window	300–700 keV	>350 keV	>140 keV	250–850 keV	250–850 keV
In-plane resolution (best nominal)	10 mm	6 mm	7 mm	5.5 mm	5.0 mm
Axial resolution (best nominal)	10 mm	12 mm	7 mm	5.0 mm	5.0 mm

*Six rings interleaved to function as 11 rings.

¹²⁴I reaction was achieved using 15 MeV deuterons incident on a 10–13 mg/cm² thick target of 96% isotope enrichment ¹²⁴Te (27). The production rate of ¹²⁴I under the conditions used was 18.5 MBq/μA h (0.5 mCi/μA h) at the end of bombardment.

Phantoms

Two basic phantoms were used (Fig. 2). The first (28) consisted of a polystyrene cylinder, 20 cm in diameter and 10 cm in thickness, which accepts and provides an appropriate scattering and attenuating environment for, various inserts. Line source inserts were used for spatial resolution measurements. Cylindrical inserts, 26 mm diameter and 8 cm active length, (actually 60 ml syringes) were used for regional count rate linearity measurements. These inserts extended uniformly through several slices of any of the scanners and were fillable with activity. The other phantom was one widely used in SPECT, commonly referred to as a "Jaszczak" phantom (Data Spectrum Corporation, Hillsborough, NC). This is a 22-cm diameter cylinder, fillable with activity and containing various combinations of fillable spheres (0.5 ml to 20 ml in volume).

Image Display and Analysis Systems

To reduce the variability in the image display and analysis systems, a common system, the National Institute of Health's MIRAGE system was used. This was implemented on both a Microvax II computer using a Lexidata display terminal and a Vaxstation (Digital Equipment Corporation, Maynard, MA). Im-

ages were reconstructed on the scanners themselves using the parameters (filter function, field of view, pixel size, etc.) and corrections (detector homogeneity, deadtime, random coincidences, attenuation correction) usually used for clinical studies at that site. Wherever possible, region of interest (ROI) analysis was done first on the data analysis system of the scanner itself and then confirmed on the Mirage system.

Parameters Measured and Methods of Measurement

Spatial Resolution. Spatial resolution was measured using ¹²⁴I in plastic tubing inserted into the 20 cm polystyrene phantom (Fig. 2A) so that any positron range effects would be included in the measurements. Acquisition and reconstruction parameters were similar to those used clinically and for imaging other phantoms in this study (Table 2). A Hanning filter was used. The plastic tubing, 1 mm internal diameter, filled with activity, was inserted in a direction perpendicular to the scan plane at the center of the polystyrene phantom. The tubing was looped back through the phantom at 20 mm intervals to provide a distance calibration. After imaging and reconstruction, a profile was drawn through the image of the line (or point, as it appears in the slice).

Linearity of Regional Observed Count Rate with Activity. The ability to make quantitative measurements of regional activity was investigated using the same polystyrene phantom with fillable cylindrical inserts (Fig. 2B). Each cylinder was filled with a different concentration of ¹²⁴I covering a 10:1 range. In a typical

TABLE 2
Acquisition and Reconstruction Parameters Used for Imaging Phantoms

	PC4600	Posicam	SP3000	ECAT 931	ECAT 951
Sphere concentration	0.15 MBq/ml	0.14 MBq/ml	0.14 MBq/ml	0.15 MBq/ml	0.15 MBq/ml
Background concentration	0.016 MBq/ml	0.014 MBq/ml	0.013 MBq/ml	0.015 MBq/ml	0.016 MBq/ml
Scan time	30 m	30 m	45 m	30 m	60 m
Detector motion	Wobbled	Wobbled	Wobbled	Non-wobbled	Non-wobbled
Matrix size	128 ²	256 ²	216 ²	128 ²	128 ²
Field of view	24 cm	47 cm	48 cm	28 cm	45 cm
Fraction of field shown	Full field	Partial field	Partial field	Full field	Partial field
Reconstruction filter	Hanning	Hanning	Hanning	Hanning	Ramp
Attenuation correction	Analytic	Analytic	Measured	Analytic	Measured
Deadtime correction	Singles based	Singles based	None	Singles based	Singles based
Randoms correction	Singles based	Singles based	Edge-of-field count based	Delayed coincidence based	Delayed coincidence based

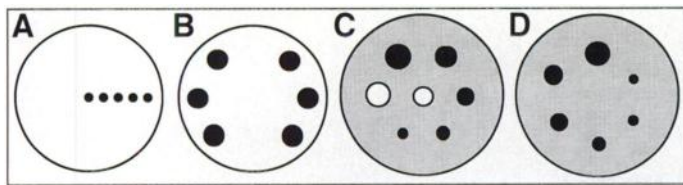


FIGURE 2. (A) Spatial resolution phantom with line source inserts. (B) Quantitation linearity phantom with six fillable cylinders (shown black). (C) Jaszczak head phantom with five fillable spheres (shown black) and two inactive spheres (shown white). The background region (shown shaded) is also fillable. (D) Jaszczak head phantom with six fillable spheres (shown black) and fillable background region (shown shaded).

measurement, the concentrations ranged from approximately 0.015–0.15 MBq/ml (0.4–4 μ Ci/ml), about 0.9–9 MBq (24–240 μ Ci) per cylinder or about 30 MBq (0.8 mCi) in the whole phantom. Acquisition and reconstruction parameters were again similar to those used clinically and for imaging the other phantoms in this study (Table 2).

Linearity was measured by determining the counts in a small ROI placed within each cylinder in the resulting images and plotting counts against concentration based on dose calibrator measurements.

Visualization and Quantitation of Activity in Spherical Objects within a 22-cm Diameter Cylindrical Phantom. Hot Spheres in Cold Background and Hot Spheres in Warm Background. To simulate conditions more likely to be encountered in humans when imaging radiolabeled antibodies, imaging was carried out with ^{124}I filled spheres of various sizes positioned within the 22-cm diameter fillable phantom. The spheres were filled with ^{124}I at the same concentration, approximately 0.15 MBq/ml (4 μ Ci/ml). This represented a total activity of about 6 MBq (160 μ Ci), confined to a few slices. The body of the phantom was filled with water. This phantom was imaged using the acquisition and reconstruction parameters given in Table 2. The measurement was then repeated with 0.015 MBq/ml (0.4 μ Ci/ml) of ^{124}I in the body of the cylinder. This represented an additional activity of about 6 MBq (160 μ Ci) per 10 mm slice, and about 95 MBq (2.6 mCi) in the whole phantom.

Mean counts were determined for ROIs placed over the spheres in the resultant images.

Image Reconstruction

In all cases, image reconstruction was done using the scanner's standard clinical protocol, typically a Hanning filter, with standard random and deadtime corrections. The attenuation correction was variously analytical or based on transmission measurements with a ring source or orbiting rod source.

RESULTS

Spatial Resolution

The resolution measurements made with ^{124}I are given in Table 3. The results obtained are consistent with what is to be expected under these acquisition and reconstruction conditions, with a slight degradation due to the higher energy and consequent

TABLE 3

Resolution of Various Scanners Using a Polyethylene-Encased Line Source of Iodine-124 in a 20-cm Polystyrene Phantom and Imaging Reconstruction Filters

Scanner model	In plane resolution FWHM
PC4600	13.5 mm
POSICAM	8 mm
SP3000	8 mm
ECAT 931	8.5 mm

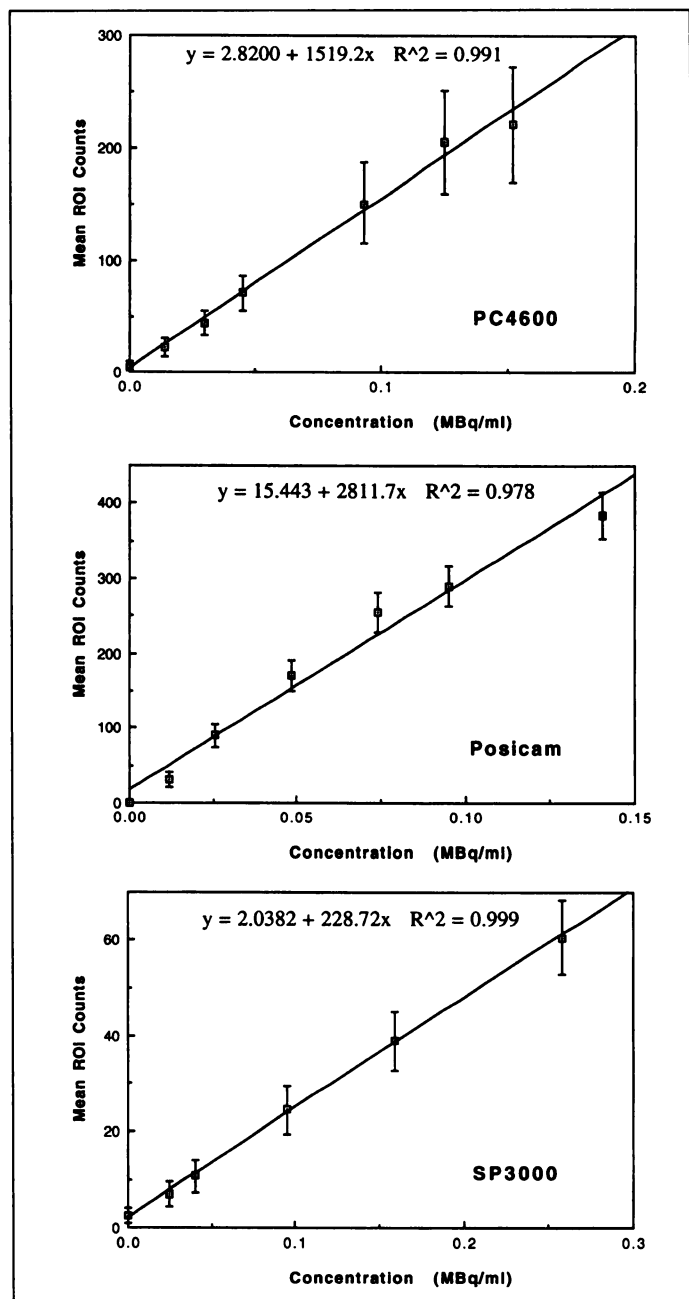


FIGURE 3. Linearity of regional observed count rate with activity measured using the quantitation linearity phantom shown in Figure 2B. Plots of observed counts within a region of interest in the image versus activity concentration based on dose calibrator measurements.

longer range of ^{124}I positrons. Resolutions quoted by manufacturers are usually measured with a lower-energy positron emitter encased in a metal tube and using a sharper reconstruction filter.

Linearity of Regional Observed Count Rate with Activity

The results of these measurements are shown in Figure 3, which compares observed counts within a ROI in the image to activity concentration. Within experimental accuracy, the plots are fairly linear. Least squares fits are shown. Thus, at these total activity levels, neither deadtime nor additional true or accidental coincidence effects involving the gamma rays of ^{124}I cause significant reduction in the ability to quantitate activity in a region due to nearby regions containing similar or higher levels of activity. The small background count seen in regions of zero activity is probably due to "true" coincidences involving either scattered annihilation photons or gamma ray photons.

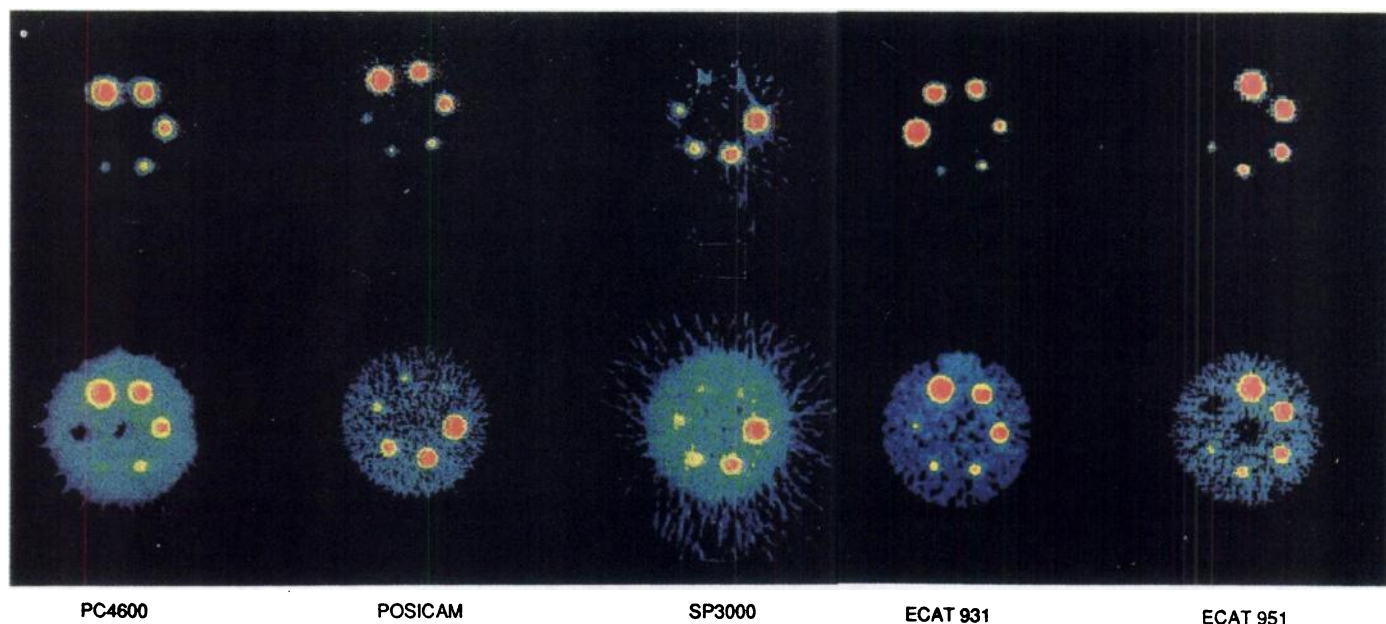


FIGURE 4. Scans of 22-cm diameter Jaszczak phantom with ^{124}I -containing "hot" spheres of various sizes in a "cold" background (upper row) and the same "hot" spheres in a "warm" background of one-tenth the concentration (lower row). The acquisition and reconstruction parameters used are given in Table 2. The choice of different parameters could affect the appearance of the image. Some phantoms also contain two "cold" spheres. Comparative counts are given in Table 4.

Visualization and Quantitation of Activity in Spherical Objects in a 22-cm Diameter Cylindrical Phantom

Figure 4 shows the results of imaging hot spheres in a cold background and the same hot spheres in a warm background. Note that while the same sphere configuration was used for a given scanner, two arrangements of spheres were used in this study (Fig. 2). Generally, all the hot spheres are visible whether or not background activity is present, although in some cases they are more clearly visible than in others. For both backgrounds, the counts observed within the large spheres are

similar (Table 4). Due to the expected partial volume effects (29–31), the counts within the smaller spheres are less than for the larger spheres, even though the concentrations are the same. Similarly, the counts are higher when these smaller spheres are in a warm background rather than a cold background due to a contribution from the surrounding activity. For two scanners, there is a trend for the counts in the large spheres to be slightly less when in a warm rather than cold background. This could be due to one or two reasons: a deadtime correction that is too small or a random correction that is too big.

TABLE 4

Mean Counts and Standard Deviation of Counts within a ROI in the Center of the Same Hot Spheres in a Cold Background (H/C) and Warm Background (H/W) for the Images Shown in Figure 4*

Diameter (mm)	Volume (cm ³)	PC4600				POSICAM				SP3000			
		H/C		H/W		H/C		H/W		H/C		H/W	
		Mean	s.d.	Mean	s.d.	Mean	s.d.	Mean	s.d.	Mean	s.d.	Mean	s.d.
33.7	20.0	100	2.1	88.3	2.7	100	5.7	102.7	5.5	100	2.4	102.4	4.9
28.2	11.8	91.9	4.3	82.2	3.4	86.9	5.9	105.8	4.9	92.9	3.9	91.5	4.6
21.9	5.5	65.6	6.6	66.0	4.3	85.3	3.7	95.7	7.8	83.4	3.7	80.2	8.5
15.6	2.0	45.9	4.9	40.7	4.5	51.5	7.3	50.6	6.0	47.4	4.5	52.8	4.9
12.4	1.0	—	—	—	—	30.7	5.4	38.8	6.0	24.3	3.2	35.5	2.7
9.8	0.5	11.2	2.1	22.4	2.0	25.8	5.7	23.9	7.3	14.6	2.9	34.7	5.2
Bkgd		0.8	0.7	16.7	1.7	0.0	3.8	8.6	5.3	3.6	1.4	16.6	3.2

Diameter (mm)	Volume (cm ³)	ECAT 931				ECAT 951			
		H/C		H/W		H/C		H/W	
		Mean	s.d.	Mean	s.d.	Mean	s.d.	Mean	s.d.
33.7	20.0	100	1.2	94.7	1.5	100	4.4	108.7	9.4
28.2	11.8	98.7	4.0	88.3	3.7	95.8	4.4	100.0	3.3
21.9	5.5	82.7	3.4	53.3	2.2	85.1	9.8	92.5	4.0
15.6	2.0	52.5	5.0	46.5	4.2	60.4	11.2	65.4	10.4
12.4	1.0	33.8	5.0	36.6	6.3	—	—	—	—
9.8	0.5	21.1	3.3	27.0	2.9	21.5	13.2	40.7	13.3
Bkgd		0.2	1.2	10.7	1.9	—	—	17.5	5.8

*For each scanner, counts are normalized to 100 percent over the largest sphere in a cold background.

When looking at the counts observed for the much lower background activity within the phantom compared with the counts for the largest spheres, the agreement is somewhat less satisfactory. Two scanners gave close to the expected result, approximately 10%, but three gave 17%.

DISCUSSION

Because only about 23% of the decays of ^{124}I result in positron emission, the number of annihilation photons per decay available for imaging is low. The positrons are of relatively high energy, which degrades spatial resolution. The many high-energy gamma rays can result in both primary and scattered photons being detected as single events within the 51-keV energy window, thus increasing the accidental coincidence count and potentially affecting quantitation (32). Furthermore, half of the positron emissions have a 603-keV gamma ray in cascade permitting "true" detected coincidences between the gamma ray and one or both of the annihilation photons. Because, however, the direction of these gamma rays has no correlation with the annihilation photons, the recorded line of coincidence is generally incorrect. Similarly, one can get undesirable "true" coincidences between cascade gamma transitions.

The PC4600 scanner used in an earlier phantom study of quantitative imaging of ^{124}I is a small diameter neurological unit with 3-mm thick, 13-cm deep tungsten septa and relatively large BGO detectors. The other scanners (Table 1) used in the present study are very different. They have larger ring diameters and axial fields of view, together with septa, which are generally shorter and thinner. This will tend to increase the probability of coincidences between annihilation photons and gamma rays or between two gamma rays. This is generally also true of the higher order cross planes used on some scanners. With smaller crystals and better spatial resolution, one would expect a scanner to be more sensitive to degradation in spatial resolution. Some scanners use detector materials other than BGO. Barium fluoride is used to enable time-of-flight measurements. Finally, the different types of correction schemes used by the various scanners will have different sensitivities to the effects of the gamma rays and additional coincidences. These differences in design were introduced to improve performance with positron emitters that have no (or little) associated gamma emission. Some of these changes, however, could potentially degrade performance with ^{124}I .

The results demonstrate that quantitative imaging with ^{124}I does seem to be possible with each of the scanners investigated, generally with only minor degradation in quality.

Apart from the statistical effects of the reduced number of annihilation photons produced per disintegration, the minor degradation in overall image quality is probably due to a combination of increased positron range, an increased number of photons which can cause random coincidences, and spurious "true" coincidences between annihilation photons and gamma rays or between two cascade gamma rays. While these factors do not appear to be significant enough to prevent quantitation, they may have some effect.

In clinical use, the relatively low positron abundance of ^{124}I may sometimes be compensated for in other ways. For example, the ratio of tumor-to-surrounding tissue will typically be higher in an antibody scan than in an ^{18}F FDG brain scan. Furthermore, as the half-life of ^{124}I is long and the biological processes of interest involving antibodies are generally fairly slow it will usually be possible to increase the imaging time. If the patient is receiving radioimmunotherapy it may also be possible to increase the administered activity. From this standpoint, it should be noted that, depending on the particular antibody and

organ involved, radiation doses from ^{124}I are typically 0.5 to 2.5 times the corresponding doses from ^{131}I (33,34).

The effect of increased positron range is simply to degrade the spatial resolution somewhat. The primary impact of this is to increase the minimum size of volume that can be quantitated with full recovery. Secondly, there will be an increased contribution to small volumes surrounded by relatively high activity.

All scanners have a means of correcting for random coincidences and it is irrelevant whether the detected events are annihilation photons or gamma rays. The increased number of photons which can cause random coincidences will have an effect only if the correction is not accurate. For the delayed coincidence correction scheme, the statistical noise will be increased. Random coincidence corrections based on singles rates or on edge-of-field counts will be just as accurate with ^{124}I as with conventional nuclides.

True coincidences between annihilation photons and gamma rays or between two cascade gamma rays will have the effect of creating a relatively uniform "background" of erroneous counts. The count distribution will not be exactly uniform. For a uniform distribution of activity, the counts will be somewhat higher in the center of the field for reasons of geometric sensitivity. There will also be a slight dependence on activity distribution. This background will not be corrected by the random coincidence correction schemes based on delayed coincidences or singles rates. However, it may be corrected by corrections based on edge-of-field counts. This could readily be added to scanners that do not have such a correction, either in addition to or in place of, the existing random coincidence correction scheme.

CONCLUSION

Phantom measurements indicate that, for tumor-like objects containing ^{124}I , surrounded by a large volume of relatively low background activity, and with other activity-containing "tumors" or "organs" nearby, quantitative measurements of activity within those tumor-like objects and the surrounding regions can be made using PET. Such measurements would appear to be feasible using scanners of very different designs, representing most of those currently commercially available.

The imaging conditions and activity concentrations used simulate those expected clinically with radiolabeled antibody imaging and various other procedures. Measurement of warm activity areas near to or surrounded by large hot areas would be expected to be more difficult, as it is even for pure positron and single gamma emitters. This was not investigated here.

Thus, under clinically relevant conditions, quantitative imaging using ^{124}I and PET appears to be possible. The ability to quantitatively image labeled antibodies over several days using PET could have important implications for accurate dosimetry in radioimmunotherapy. Preliminary studies on patients using this approach have been reported elsewhere (17,20).

ACKNOWLEDGMENTS

We express our appreciation to R. Weise and J. Horst for help with the measurements on the ECAT 951, to Positron Corp. for help with the measurements on their scanner and to Siemens for help in arranging shipment of ^{124}I and phantoms in Germany. This work was supported in part by U.S. Department of Energy contract DE-FG02-86ER60407. J.S.K. was supported in part by U.S. Department of Energy contract DE-FG02-88ER60642.

REFERENCES

1. Thomas SR, Maxon HR III, Kereiakes JG. Techniques for quantitation of in vivo radioactivity. In: Gelfand MJ, Thomas SR, eds. *Effective use of computers in nuclear medicine*. New York: McGraw-Hill; 1988:468-484.

2. Leichner PK, Klein JL, Garrison JB, et al. Dosimetry of I131-labeled antiferritin in hepatoma: A model for radioimmunoglobulin dosimetry. *Int J Radiat Oncol Biol Phys* 1981;7:323-333.
3. Moldofsky PJ, Beardsley MR, Mulhern Jr CB. External imaging techniques for quantitation of distribution of I-131 F(ab')₂ fragments of monoclonal antibody in humans. *Med Phys* 1984;11:778-783.
4. Zanzonico PB, Bigler RE, Sgouros G, Strauss A. Quantitative SPECT in radiation dosimetry. *Semin Nucl Med* 1989;19:47-61.
5. Chang LT. A method for attenuation correction in radionuclide computer tomography. *IEEE Trans Nucl Sci* 1978;NS25:638-643.
6. Jaszcak RJ, Greer KL, Coleman RE. SPECT. In: Rao DV, Chandra R, Graham MC, eds. *Physics of nuclear medicine: recent advances, medical physics monograph no. 10*. New York: American Association of Physicists in Medicine; 1984:457-482.
7. Hawkins WG, Leichner PK, Yang N-C. The circular harmonic transform for SPECT reconstruction and boundary conditions on the Fourier transform of the sinogram. *IEEE Trans on Med Imaging* 1988;7:135-148.
8. Weber DA, Eckerman KF, Dillman LT, Ryman JC. *MIRD: radionuclide data and decay schemes*. New York: Society of Nuclear Medicine; 1989.
9. Frey P, Townsend O, Jeavons A, Donath A. In vivo imaging of the human thyroid with a positron camera using I-124. *Eur J Nucl Med* 1985;10:472-476.
10. Miraldi F, Nelson AD, Berridge MS, Cheung N-KV. Positron imaging of neuroblastoma tumors with ¹²⁴I/¹²³I-labeled monoclonal antibody 3F8 [Abstract]. *J Nucl Med* 1987;28:1078.
11. Ott RJ, Batty V, Webb S, et al. Measurement of radiation dose to the thyroid using positron emission tomography. *Br J Radiol* 1987;60:245-251.
12. Lambrecht RM, Woodhouse N, Phillips R, et al. Investigational study of iodine-124 with a positron camera. *Am J Physiol Imaging* 1988;3:197-200.
13. Miraldi F. Monoclonal antibodies and neuroblastoma. *Semin Nucl Med* 1989;19:282-294.
14. Langen K-J, Coenen HH, Rosen N, et al. SPECT studies of brain tumors with L-3-[¹²³I]iodo-alpha-methyl tyrosine: Comparison with PET, ¹²⁴IMT and first clinical results. *J Nucl Med* 1990;31:281-286.
15. Snook DE, Rowlinson-Busza G, Sharma HL, Epenetos AA. Preparation and in vivo study of iodine-124-labeled monoclonal antibody HE17E2 in a human tumour xenograft model: a prelude to positron emission tomography (PET). *Br J Cancer* 1990;62(suppl 10):89-91.
16. Wilson CB, Snook DE, Dhokia B, et al. Quantitative measurement of monoclonal antibody distribution and blood flow using positron emission tomography and ¹²⁴I in patients with breast cancer. *Int J Cancer* 1991;47:344-347.
17. Westera G, Reist HW, Buchegger F, et al. Radioimmuno positron emission tomography with monoclonal antibodies: a new approach to quantifying in vivo tumour concentration and biodistribution for radioimmunotherapy. *Nucl Med Commun* 1991;12:429-437.
18. Larson SM, Pentlow KS, Volkow ND, et al. PET scanning of ¹²⁴I 3F8 as a novel approach to tumor dosimetry during treatment planning for radioimmunotherapy in a child with neuroblastoma. *J Nucl Med* 1992;33:2020-2023.
19. Bakir MA, Eccles SA, Babich JW, et al. c-erbB2 protein overexpression in breast cancer as a target for PET using iodine-124-labeled monoclonal antibodies. *J Nucl Med* 1992;33:2154-2160; 1993;34:290 [Erratum].
20. Rubin SC, Kairemo KJA, Brownell AL, et al. High-resolution positron emission tomography of human ovarian cancer in nude rats using ¹²⁴I-labeled monoclonal antibodies. *Gynecol Oncol* 1993;48:61-67.
21. Daghighian FD, Pentlow KS, Larson SM, et al. Development of a method to measure kinetics of radiolabeled monoclonal antibody in human tumor with applications to microdosimetry: positron emission tomography studies of iodine-124-labeled 3F8 monoclonal antibody in glioma. *Eur J Nucl Med* 1993;20:402-409.
22. Pentlow KS, Graham MC, Lambrecht RM, Cheung N-KV, Larson SM. Quantitative imaging of I-124 using positron emission tomography with applications to radioimmunodiagnosis and radioimmunotherapy. *Med Phys* 1991;18:357-366.
23. Kearfott K, Carroll LR. Evaluation of the performance characteristics of the PC4600 positron emission tomograph. *J Comput Assist Tomogr* 1984;8:502-513.
24. Batchelor S, Blake GM, Saunders JE. A comparison of three commercially available PET imaging systems. *Nucl Med Commun* 1992;13:20-27.
25. Wellen TK, Bice AN, Harrison RL, Pencke MD, Link JM. Performance measurements of the SP3000/UW time-of-flight positron emission tomograph. *IEEE Trans Nucl Sci* 1988;NS-35:665-669.
26. Spinks TJ, Jones T, Gilardi MC, Heather JD. Physical performance of the latest generation of commercial positron scanner. *IEEE Trans Nucl Sci* 1988;NS-35:721-725.
27. Clem RG, Lambrecht RM. Enriched ¹²⁴Te targets for production of ¹²³I and ¹²⁴I. *Nucl Instrum Meth Phys Res* 1991;A303:115-118.
28. Bigler RE, Yoshizumi T, Graham MC. Positron instrumentation: intercomparison measurements, specifications, test procedure, figure of merit optimization, scatter measurements. In: Rao DV, Chandra R, Graham MC, eds. *Physics of nuclear medicine: recent advances, medical physics monograph no. 10*. New York: American Association of Physicists in Medicine; 1984:411-441.
29. Hoffman EJ, Huang SC, Phelps MJ. Quantitation in positron emission computed tomography: effect of object size. *J Comput Assist Tomogr* 1979;3:299-308.
30. Kessler RM, Ellis JR, Eden M. Analysis of emission tomographic scan data: limitations imposed by resolution and background. *J Comput Assist Tomogr* 1984;8:514-522.
31. Spinks TJ, Guzzardi R, Bellina CR. Performance characteristics of a whole-body positron tomograph. *J Nucl Med* 1988;29:1833-1841.
32. Hoffman EJ, Huang SC, Phelps ME, Kuhl DE. Quantitation in positron emission computed tomography: 4: effect of accidental coincidences. *J Comput Assist Tomogr* 1981;5:391-400.
33. Snyder WS, Ford MR, Warner GG, Watson SB. "S," Absorbed dose per unit cumulated activity for selected radionuclides and organs. *MIRD Pamphlet No. 11*. New York: Society of Nuclear Medicine; 1975.
34. Berman M, Braverman LE, Burke J, DeGroot L, McCormack KR, Oddie TH, Rohrer RH, Wellman HN, Smith EM. MIRD/dose estimate report no. 5: summary of current radiation dose estimates to humans from ¹²³I, ¹²⁴I, ¹²⁵I, ¹²⁶I, ¹³⁰I, ¹³¹I, ¹³²I as sodium iodide. *J Nucl Med* 1975;16:857-860.

Stereotactic Coordinates from ECT Sinograms for Radionuclide-Guided Breast Biopsy

Raymond R. Raylman, Edward P. Ficaro and Richard L. Wahl

Department of Internal Medicine and Division of Nuclear Medicine, Department of Radiology, University of Michigan Medical Center, Ann Arbor, Michigan

Raw data from emission scanners contained in ECT sinograms can provide an abundance of information about the position of an object in the camera's field-of-view. Since some cancers can be detected by PET and SPECT which are not seen clearly on mammograms, CT or other scans, sinogram data could potentially be used to guide tumor biopsy. For example, positron-emitting (¹⁸F-labeled Fluorodeoxyglucose) and single-photon emitting (^{99m}Tc-labeled-sestamibi) radiopharmaceuticals have been used successfully to detect many types of breast cancer. By utilizing some relatively simple geometric relationships, a sinogram-based method for biopsy of radiopharmaceutical-avid breast masses guided by data from PET and SPECT scanners has been developed and validated in phantom studies. **Methods:** A pair of projection views from a series of sinograms is used to calculate the position of photon-emitting objects. Calculated positions of spheres ranging in size from 1.6 to 3.4 cm diameters containing ¹⁸F and ^{99m}Tc were compared with

measured positions. By adding a single radioactive fiducial marker, emission-guided biopsy of simulated breast lesions was performed with a specially designed phantom containing photon-emitting spheres 12.7 mm in diameter. **Results:** Correlation between calculated and measured object coordinates were excellent (R = 1.0, R = 1.0 and R = 0.998; x, y and z coordinates, respectively). The maximum error in localization was ±3 mm. One hundred percent (10 of 10) of the attempted biopsies of simulated tumors were successful. **Conclusion:** A method for rapidly determining the position of photon-emitting objects in an emission scanner has been developed and tested. This technique, which does not require standard emission or anatomic images, could be used with dedicated biopsy machines or incorporated into "add-on" biopsy devices for existing PET or SPECT cameras.

Key Words: fluorine-18-FDG; technetium-99m-sestamibi; stereotactic biopsy; needle biopsy; breast cancer; emission computed tomography

J Nucl Med 1996; 37:1562-1567

Received Sept. 29, 1995; revision accepted Feb. 9, 1996.

For correspondence or reprints contact: Raymond R. Raylman, Ph.D., Health Sciences Center South, West Virginia University, Radiology/PET, Box 9236, Morgantown, WV 26506-9236.